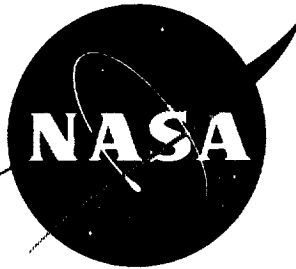


NASA TM X-258

NASA TM X-258



11-07
94-2230
245

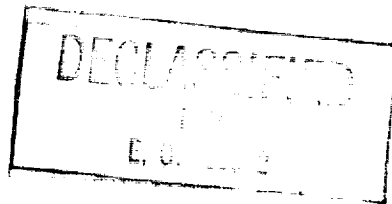
TECHNICAL MEMORANDUM

X-258

INTERNAL-PERFORMANCE EVALUATION OF A TWO-POSITION
DIVERGENT SHROUD EJECTOR

By James R. Mihalow and Andrew J. Stofan

Lewis Research Center
Cleveland, Ohio



THIS INTERIM DRAFT IS FOR
THE OFFICIAL USE OF THE
INITIAL RECIPIENT ONLY.

REVIEW
COPY

Library NASA-FRC

MAY 11 1960

CLASSIFIED DOCUMENT - TITLE UNCLASSIFIED

This material contains information affecting the national defense of the United States within the meaning of the espionage laws, Title 18, U.S.C., Secs. 793 and 794, the transmission or revelation of which in any manner to an unauthorized person is prohibited by law.

NATIONAL AERONAUTICS AND SPACE ADMINISTRATION
WASHINGTON

1947

1947

[REDACTED]

NATIONAL AERONAUTICS AND SPACE ADMINISTRATION

TECHNICAL MEMORANDUM X-258

INTERNAL-PERFORMANCE EVALUATION OF A TWO-POSITION
DIVERGENT SHROUD EJECTOR*

By James R. Mihalow and Andrew J. Stofan

ABSTRACT

A two-position divergent shroud ejector was investigated in an unheated quiescent-air facility over a range of operational variables applicable to a Mach 2.5 aircraft. The performance data are shown in terms of hypothetical engine operating conditions to illustrate variations of performance with Mach number. The overall thrust performance was reasonably good, with ejector thrust ratios ranging from 0.97 to 0.98 for all conditions except that corresponding to acceleration with afterburning through the transonic flight Mach number region from 0.9 to 1.1, where the ejector thrust ratio decreased to as low as 0.945 for an ejector corrected weight-flow ratio of 0.105.

INDEX HEADINGS

Nozzles	1.4.2.2
Exits	1.4.3
Pumps, Jet and Thrust Augmentors	1.4.4

*Title, Unclassified.

[REDACTED]

• •

• •

[REDACTED]

NATIONAL AERONAUTICS AND SPACE ADMINISTRATION

TECHNICAL MEMORANDUM X-258

INTERNAL-PERFORMANCE EVALUATION OF A TWO-POSITION
DIVERGENT SHROUD EJECTOR*

By James R. Mihalow and Andrew J. Stofan

SUMMARY

A quiescent-air internal-performance evaluation was conducted on 0.3-scale models of a two-position divergent shroud ejector applicable to operation at flight Mach numbers up to 2.5. The shroud positions corresponded to those used under typical turbojet nonafterburning and afterburning operating conditions. A series of fixed scale models simulating maximum afterburning takeoff, maximum afterburning acceleration, partial afterburning cruise, and nonafterburning cruise were evaluated. The investigation was conducted with dry unheated air over a range of primary pressure ratios to 23 and ejector corrected weight-flow ratios to 0.10. The ejector thrust ratio was between 0.97 and 0.98 over the entire range of operating conditions except for acceleration with afterburning through the Mach number region from 0.9 to 1.1, where it decreased to as low as 0.945 for an ejector corrected weight-flow ratio of 0.105.

INTRODUCTION

Off-design performance of aircraft ejectors is frequently an important consideration in the design of supersonic aircraft, especially if the aircraft is also required to cruise at high subsonic speeds. For such cases, various ejector configurations ranging from fixed to continuously variable shrouds have been considered (refs. 1 to 3). Fixed-shroud ejectors designed for good performance at high supersonic speeds usually suffer at the lower speeds because of overexpansion, although a satisfactory overall compromise can sometimes be accomplished. On the other hand, a continuously variable shroud ejector will provide peak performance over a wide range of conditions; however, weight and complexity of such an ejector could outweigh the performance advantage. It seems reasonable, then, that a compromise between the fixed and continuously variable geometry may give a light, relatively simple ejector that would have good performance at certain selected off-design points as well as at the high-speed design point.

* Title, Unclassified.

This report embodies an internal-performance evaluation of such an ejector having a two-position conical-section divergent shroud with positions corresponding to nonafterburning and afterburning operation. In the afterburning position, the shroud was opened to provide longitudinal slots to improve the overexpanded performance (unpublished NASA Lewis data). The ejector design is applicable over a range of Mach numbers up to 2.5 with design points at flight Mach numbers M_0 of 0.9 and 2.5. A series of tests of fixed-scale models simulating the ejector at maximum afterburning takeoff, maximum afterburning acceleration at $M_0 = 0.9$ to 2.5, partial afterburning cruise at $M_0 = 2.0$ to 2.5, and nonafterburning cruise at $M_0 = 0.9$ were run. The tests were conducted in a facility using unheated quiescent air over a range of primary pressure ratios to 23 and ejector corrected weight-flow ratios to 0.10. The ejector thrust and pumping characteristics were defined for each configuration investigated as well as for a composite configuration over the Mach number range up to 2.5. Two models were tested with and without simulated shroud and primary-nozzle actuating mechanisms in order to determine the performance loss attributed to the blockage of these parts.

SYMBOLS

The following symbols are used in this report:

C_d	flow coefficient, ratio of actual to ideal primary mass flow
D	diameter, in.
F	gross thrust, lb
F_{ej}	measured ejector gross thrust, lb
F_{ip}	ideal primary thrust based on measured primary mass flow and one-dimensional isentropic velocity at measured primary pressure ratio, lb
F_{is}	ideal secondary thrust based on measured secondary mass flow and one-dimensional isentropic velocity at measured secondary pressure ratio, lb
L	spacing, ft (fig. 1)
M	Mach number, dimensionless
P	total pressure, lb/sq ft abs

p	static pressure, lb/sq ft abs
T	total temperature, °R
w	weight-flow rate, lb/sec
α	ejector flow angle, deg
δ	primary convergence angle, deg
θ	shroud divergence angle, deg

Subscripts:

b	base
e	exit
p	primary
s	secondary
0	ambient

Parameters:

D_e/D_p	shroud exit-diameter ratio
D_s/D_p	shroud throat-diameter ratio
$F_{ej}/(F_{ip} + F_{is})$	ejector thrust ratio
F_p/F_{ip}	primary thrust ratio
L/D_p	spacing ratio
P_p/P_0	primary pressure ratio
P_s/P_p	ejector total-pressure ratio
$(w_s/w_p) \sqrt{T_s/T_p}$	ejector corrected weight-flow ratio


APPARATUS

Ejector


The ejector configurations are described in terms of dimensionless parameters in figure 1. The models consisted of two fixed shrouds simulating afterburning and nonafterburning operation and four primary convergent nozzles. The afterburning shroud was an 11.5° -half-angle divergent slotted (fig. 2) conical section designed for an exit diameter ratio of 1.40 at a Mach number of 2.5. The nonafterburning shroud formed a 3.4° -half-angle convergent unslotted conical section designed for an exit diameter ratio of 1.11 at a Mach number of 0.9. The four longitudinal slots in the afterburning shroud (fig. 2) were spaced circumferentially at 90° intervals and opened up about 10 percent of the shroud area. The purpose of the slots was to induce flow separation and improve aerodynamic stability during conditions that otherwise would have resulted in overexpanded operation. Simulated secondary blockage, as shown in figure 3, consisted of primary cams and rings, secondary ring, and flap support cone. These parts were removable so that the performance could be evaluated with and without the blockage.

Test Setup

The test setup shown in figure 4 is the same as described in detail in previous ejector reports (e.g., ref. 4). The setup consisted of a plenum tank mounted between the laboratory high-pressure air and exhaust systems. Two labyrinth seals, installed in series at the upstream end of the mounting pipe, maintained the pressure differential across the nozzle and ejector. The tank contained a bedplate freely suspended by four flexure rods on which the ejector and mounting pipe were installed. The resultant force on the ejector and mounting pipe was transmitted through linkages to a calibrated null-type force-measuring cell.

Instrumentation

Instrumentation stations are indicated in figures 3 and 4. The description and use is given in the following table:



Station	Location	Static-pressure taps	Total-pressure tubes	Temperature thermocouples	Use
0	Ambient	4	-	-	Ambient
1	Inlet	-	4	2	Primary-inlet momentum
2	Forward bellmouth	4	-	-	Primary-inlet momentum
3	Primary-air measuring	4	12 (2 rakes)	-	Primary mass flow
4	Rear bellmouth	4	-	-	External pressure force
5	Upstream secondary orifice	1	-	-	Secondary mass flow
6	Downstream secondary orifice	1	-	-	Secondary mass flow
7	Thrust cell	-	1	-	Resultant force
p	Primary inlet	4	8 (1 rake)	-	Primary-inlet conditions
s	Secondary inlet	-	4	-	Secondary-inlet conditions

PROCEDURE

First, the four primary nozzles were run over a range of primary pressure ratios from 1.5 to 18.0 in order to determine the performance characteristics. Next, the four complete ejectors were evaluated with the simulated secondary blockage. For each ejector configuration, several ejector corrected weight-flow ratios $((w_s/w_p)\sqrt{T_s/T_p})$, where $T_s/T_p = 1.0$ for this investigation) from 0 to 0.10 were run over a range of primary pressure ratios from 0 to 23 at constant primary mass flow. The maximum afterburning and nonafterburning cruise configurations were then rerun without secondary blockage in order to evaluate the blockage losses.

Methods of calculating primary and secondary mass flow and gross thrust are basically the same as those given in appendix B of reference 4.

PRESENTATION OF DATA

Primary-Nozzle Performance

The primary thrust ratio and flow coefficient are presented for a range of primary pressure ratios for each primary nozzle in figure 5.

The thrust performance is essentially the same for all nozzles within the range of experimental accuracy, but the flow coefficients are a function of the nozzle convergence angle - as would be expected.

Ejector Performance

To illustrate the variation of ejector performance with flight Mach number, a hypothetical engine operating schedule was used - as shown in figure 6. The schedule assumed a constant inlet kinetic-energy efficiency of 95 percent and is typical of high-pressure-ratio engines operating at Mach numbers up to about 2.5.

The basic performance of each ejector configuration is given in figures 7 to 10 as plots of the following parameters against primary pressure ratio for several constant ejector corrected weight-flow ratios:

- (1) Ejector thrust ratio, $F_{ej}/(F_{ip} + F_{is})$
- (2) Ejector total-pressure ratio, P_s/P_p
- (3) Primary flow coefficient, C_d

Data for the configurations, run with and without the secondary blockage, are included in figures 8 and 10.

Pumping performance. - Pumping performance for each ejector is shown in figures 7(a) to 10(a). A curve for the maximum ejector total-pressure ratio available is also shown. This maximum was calculated from the assumed engine operating schedule, the main inlet recovery, and a secondary duct subsonic recovery of 0.95. Ejector corrected weight-flow ratios required for cooling (0.04 to 0.10) could easily be provided for all configurations except that used during maximum afterburning take-off and possibly that for maximum afterburning acceleration. This condition at a primary pressure ratio of 2.0 is marginal. The effect of the secondary blockage was to lower the pumping capacity of the ejector at the higher corrected ejector weight-flow ratios. The configurations with blockage required a 7-to-11-percent increase in the ejector total-pressure ratio to pass the same flow at an ejector corrected weight-flow ratio on the order of 0.10.

Primary flow coefficient. - The primary-nozzle flow coefficients (figs. 7(b) to 10(b)) with the shrouds in place were essentially the same as without the shrouds for all configurations except configuration 4. For this case, the flow coefficient dropped from about 0.94 to 0.93 as ejector corrected weight-flow ratio was increased from 0 to 0.107.

Thrust performance. - The thrust data presented in figures 7(c) to 10(c) are useful in defining detailed performance over a wide range of operating conditions; however, the performance at typical operating conditions is illustrated more clearly in figure 11, which is a composite graph of the ejector thrust ratio of the configurations investigated as a function of Mach number. The ejector thrust ratio obtainable at the significant operating points (takeoff, Mach 0.9 cruise, and Mach 2.5 cruise) varied approximately between 0.97 and 0.98 except for the maximum-afterburning-acceleration condition in the transonic $M_0 = 0.9$ to 1.1 region, where it decreased to 0.945 at a corrected weight-flow ratio of 0.105. The reason for this dropoff is that the flow through the ejector was overexpanded. Obviously, the performance in this region could be improved by decreasing the expansion ratio, but this would compromise the high-Mach-number design-point performance.

As compared with a continuously variable shroud ejector (ref. 2), the performance of the two-position shroud suffered only about 1 percent except in the transonic $M_0 = 0.9$ to 1.1 region, where losses are as high as 3 or 4 percent. Within experimental accuracy, no thrust losses could be attributed to the secondary blockage.

SUMMARY OF RESULTS

A two-position divergent shroud ejector design applicable to Mach numbers up to about 2.5 was evaluated over a range of primary pressure ratios and corrected ejector weight-flow ratios to determine the internal-thrust and pumping characteristics.

The overall thrust performance of the ejector was reasonably good, with ejector thrust ratios ranging from 0.97 to 0.98 at all pertinent operating conditions except that corresponding to acceleration with afterburning through the transonic (free-stream Mach 0.9 to 1.1) region, where it decreased to as low as 0.945 at an ejector corrected weight-flow ratio of 0.105. Pumping capacity would probably be sufficient for cooling at all operating conditions except possibly maximum afterburning takeoff.

No significant difference was detected between thrust performance of the ejector with or without the simulated secondary-air-passage blockage. The effect of blockage on pumping was to reduce the ejector capacity at the higher ejector corrected weight-flow ratios.

Lewis Research Center
National Aeronautics and Space Administration
Cleveland, Ohio, March 29, 1960

REFERENCES

1. Mihalow, James R.: Internal-Performance Evaluation of Two Fixed-Divergent-Shroud Ejectors. NASA TM X-257, 1960.
2. Stofan, Andrew J., and Mihalow, James R.: Performance of a Variable Divergent-Shroud Ejector Nozzle Designed for Flight Mach Numbers up to 3.0. NASA TM X-255, 1960.
3. Beheim, Milton A.: Off-Design Performance of Divergent Ejectors. NACA RM E58G10a, 1958.
4. Trout, Arthur M., Papell, S. Stephen, and Povolny, John H.: Internal Performance of Several Divergent-Shroud Ejector Nozzles with High Divergence Angles. NACA RM E57F13, 1957.

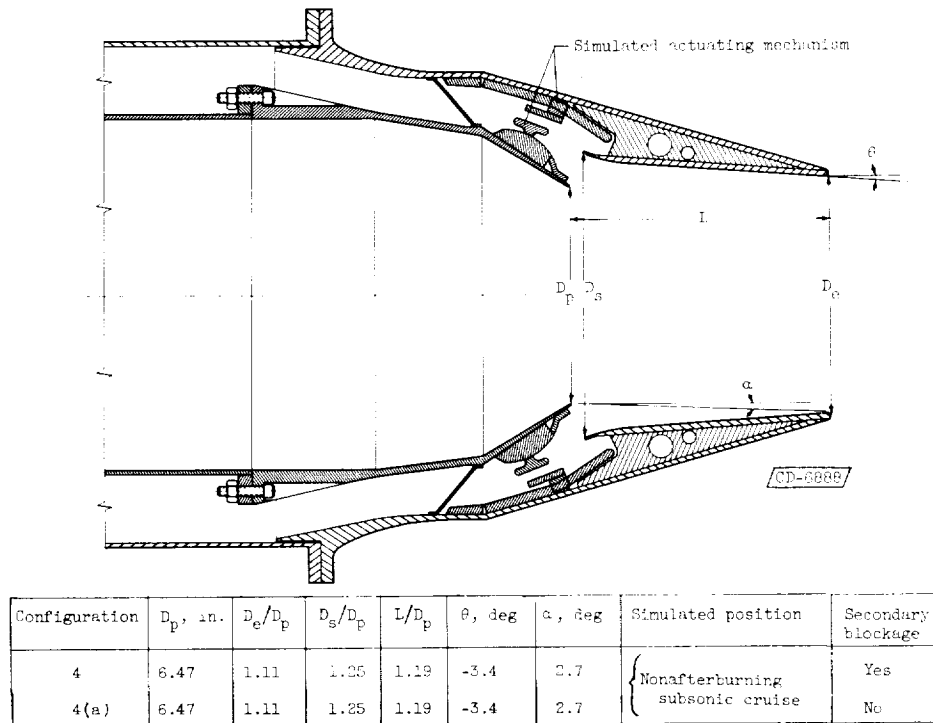
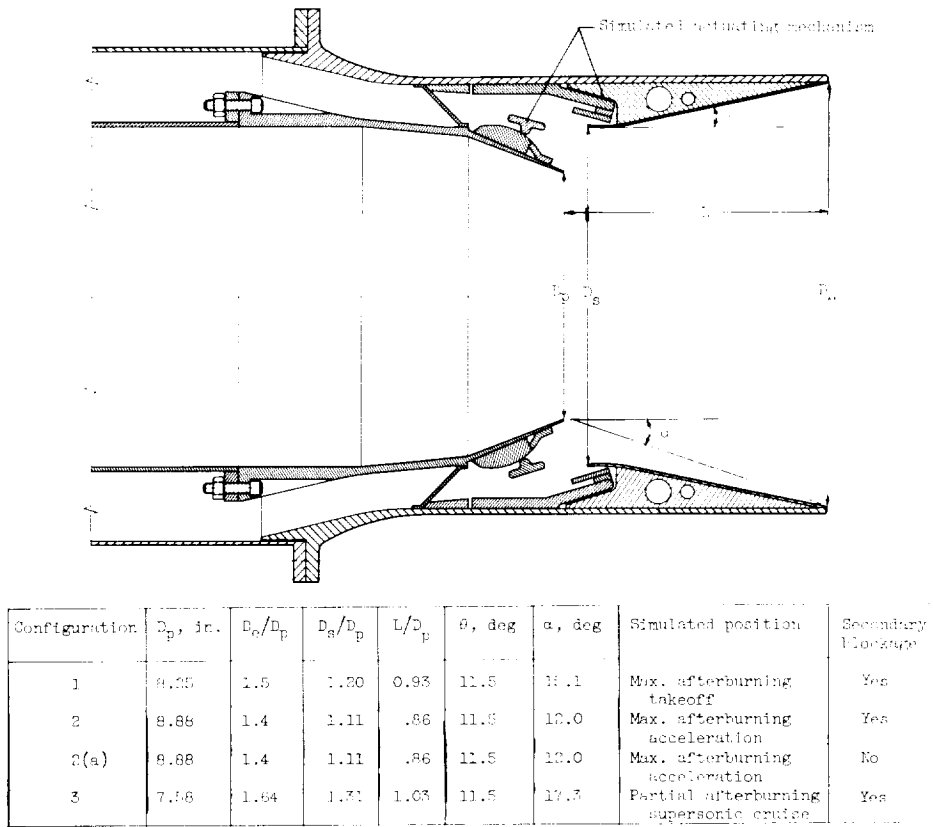
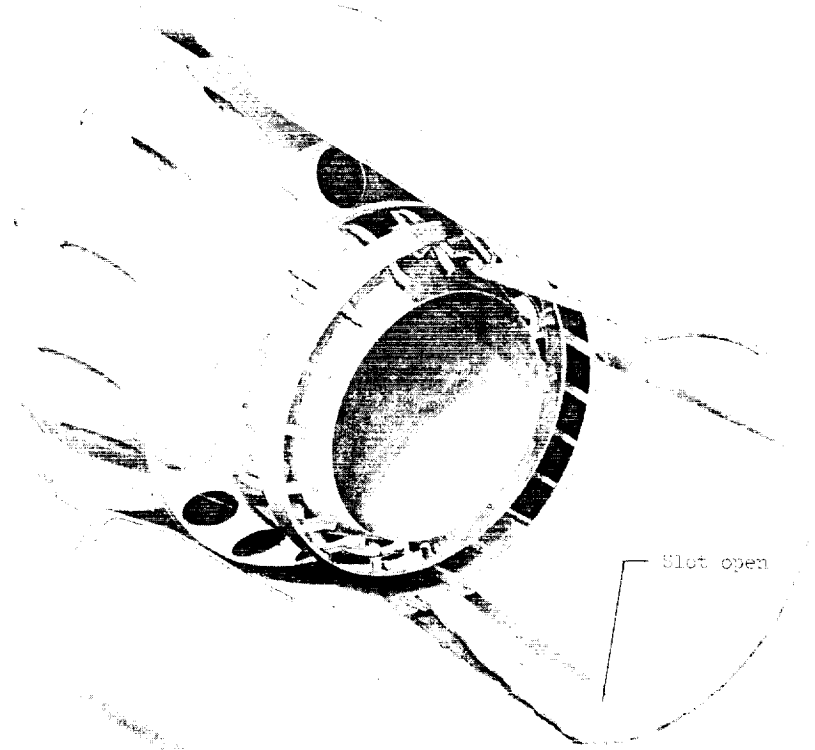
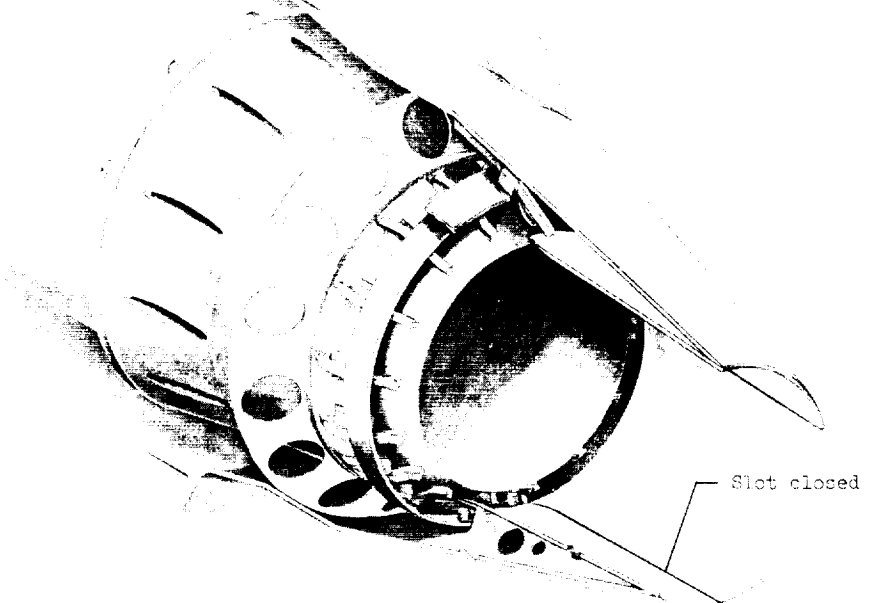


Figure 1. - Ejector configurations and dimensions.



(a) Afterburning position.



(b) Nonafterburning position.

CD-6314

Figure 2. - Ejector cutaway showing longitudinal slots.

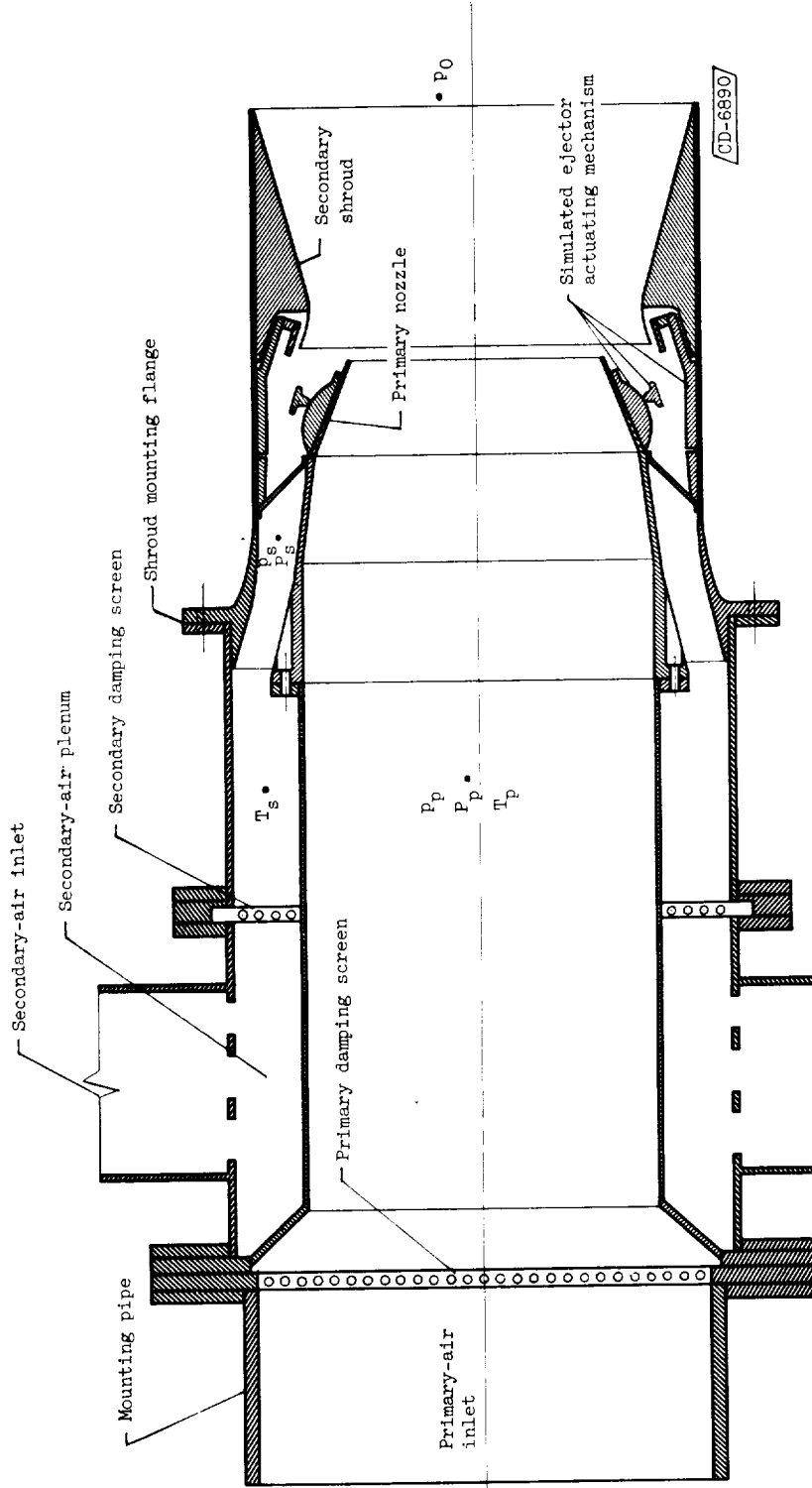


Figure 3. - Ejector and instrumentation location.

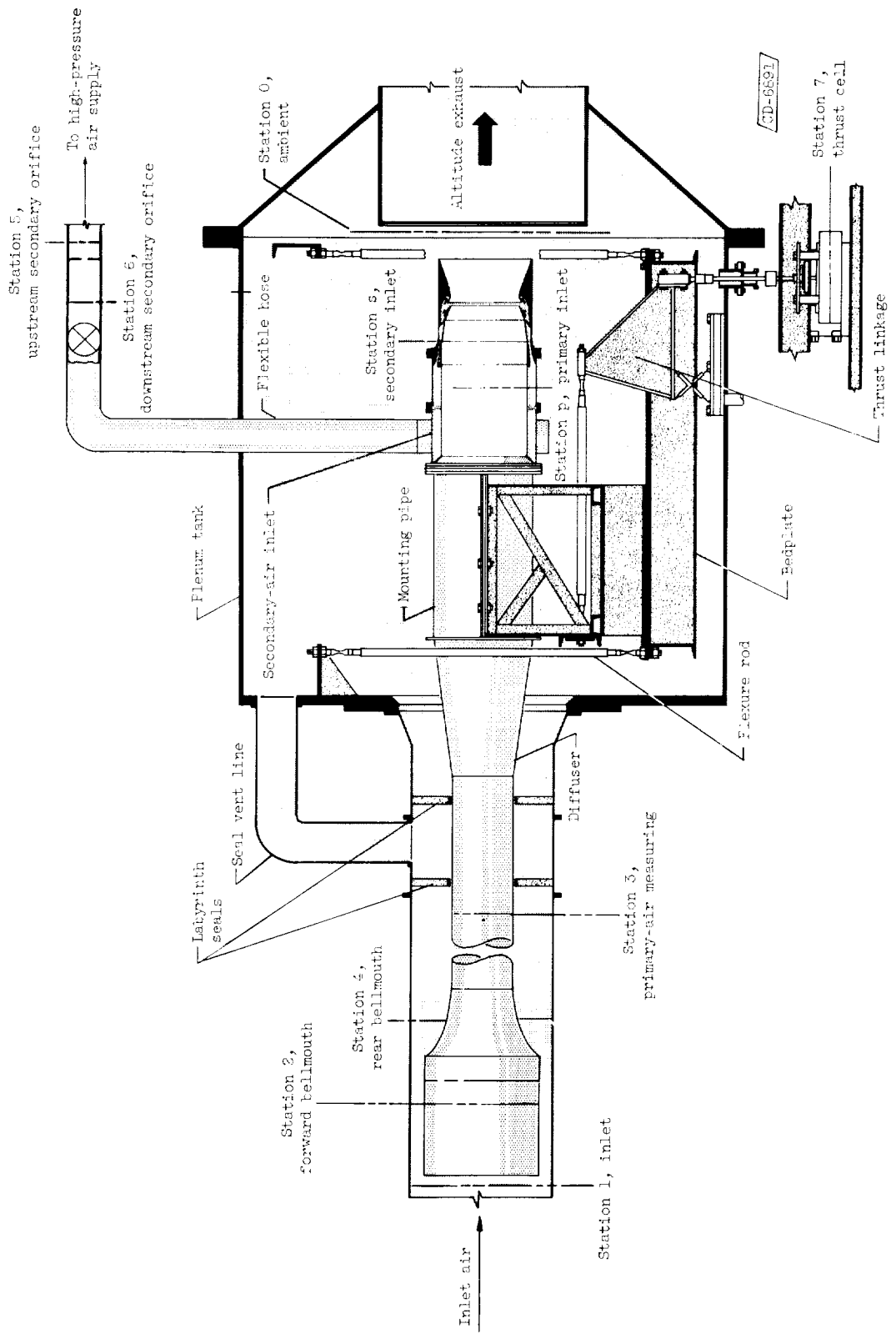
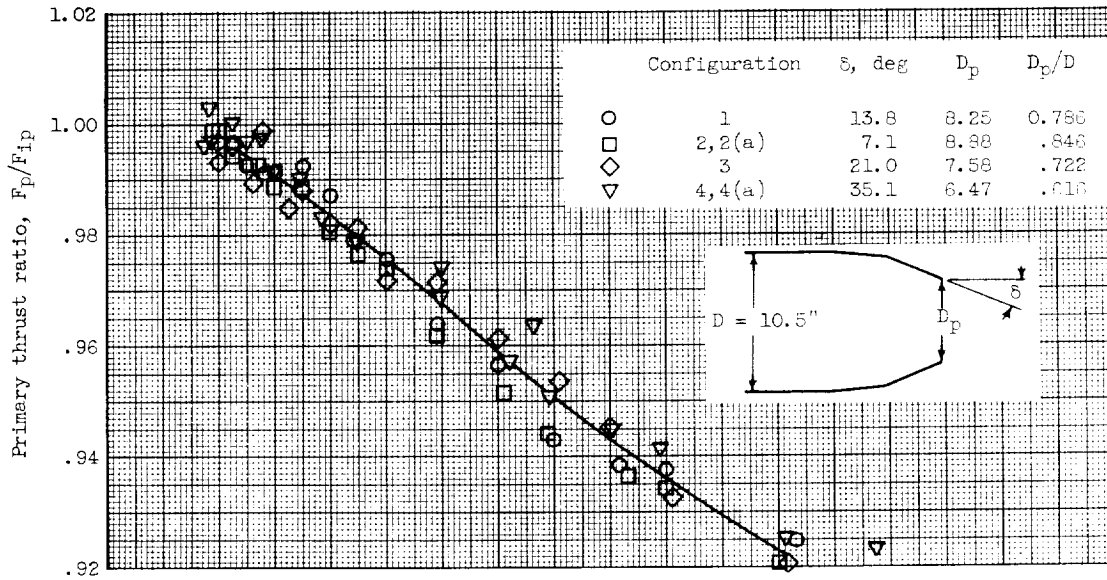
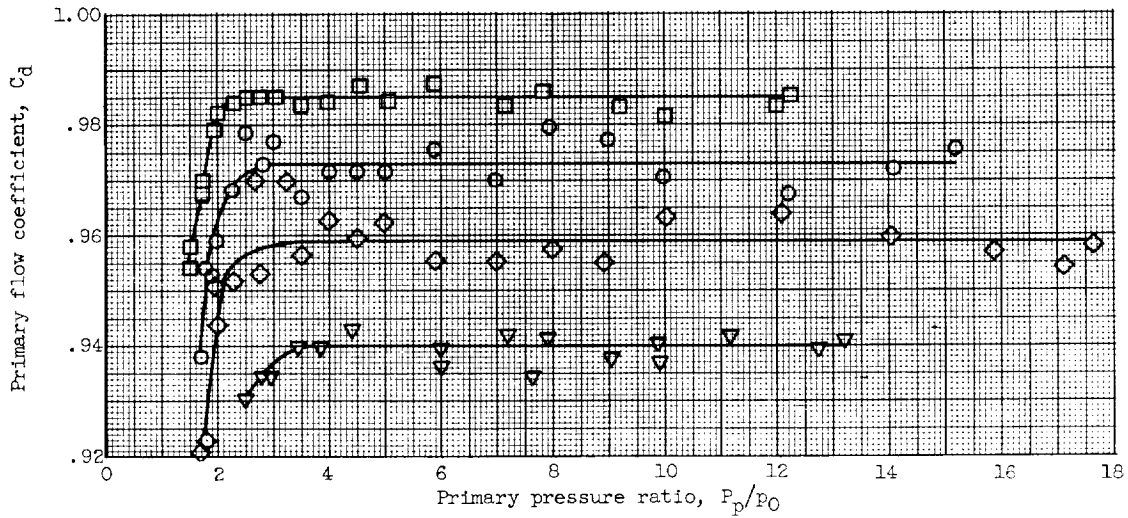


Figure 4. - Test setup and station locations.

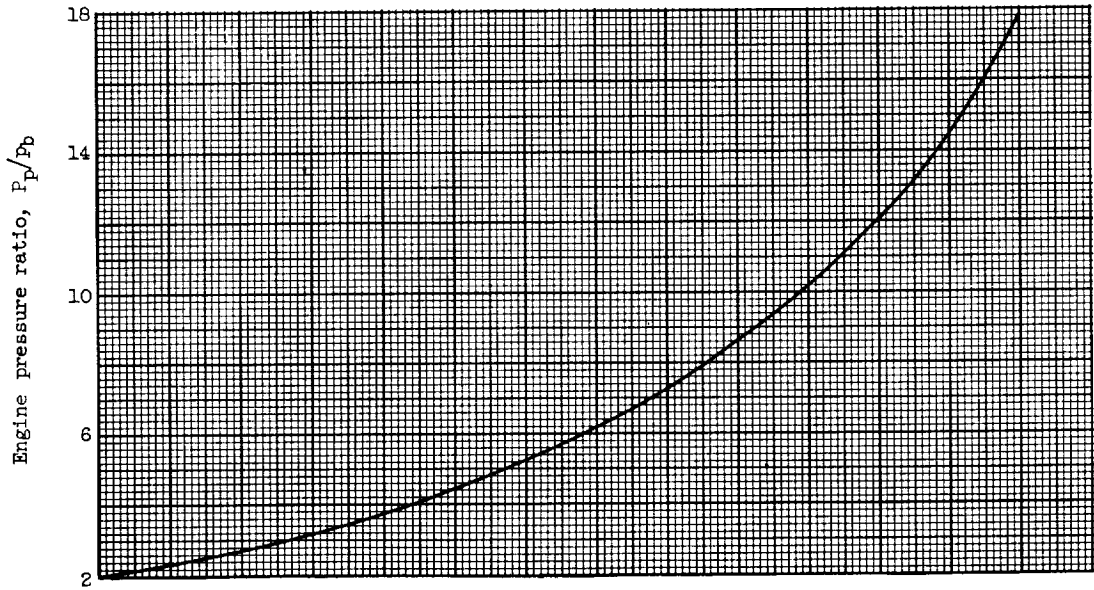


(a) Thrust performance.

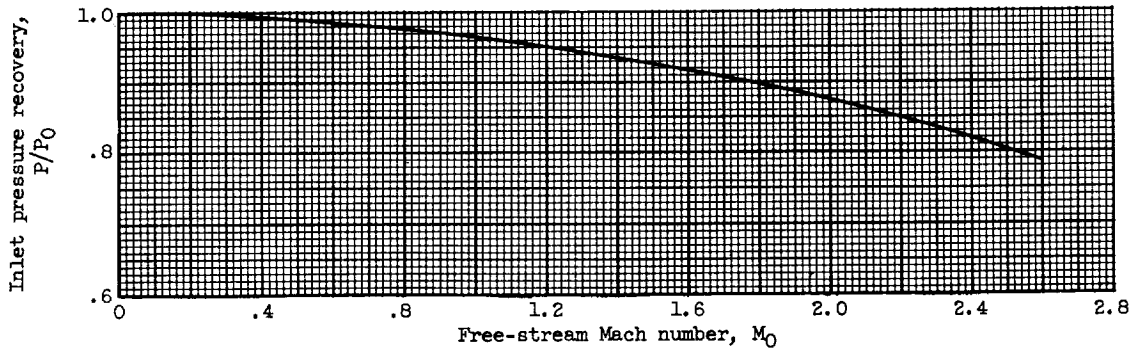


(b) Flow performance.

Figure 5. - Performance of primary nozzles.



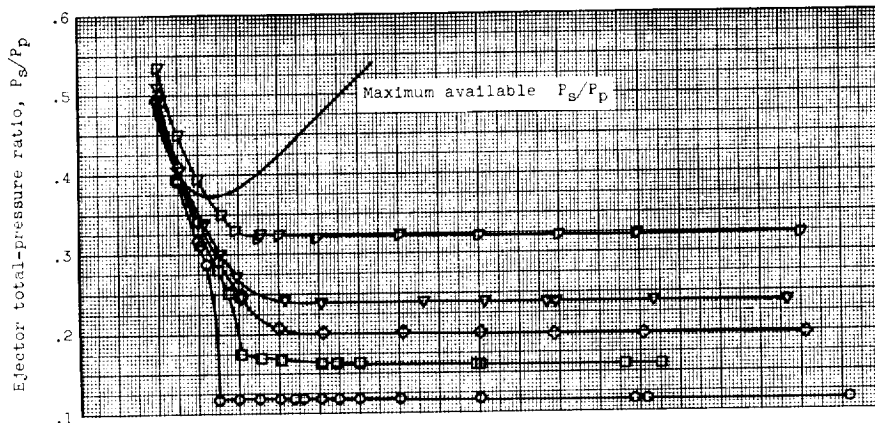
(a) Nozzle operating schedule.



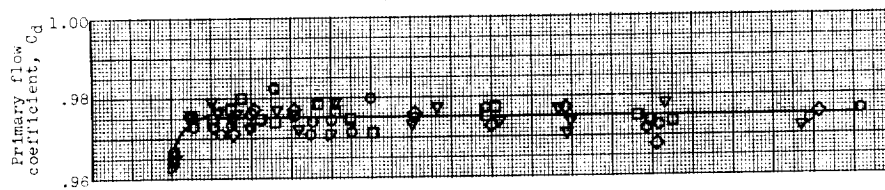
(b) Inlet recovery.

Figure 6. - Assumed engine operating schedule.

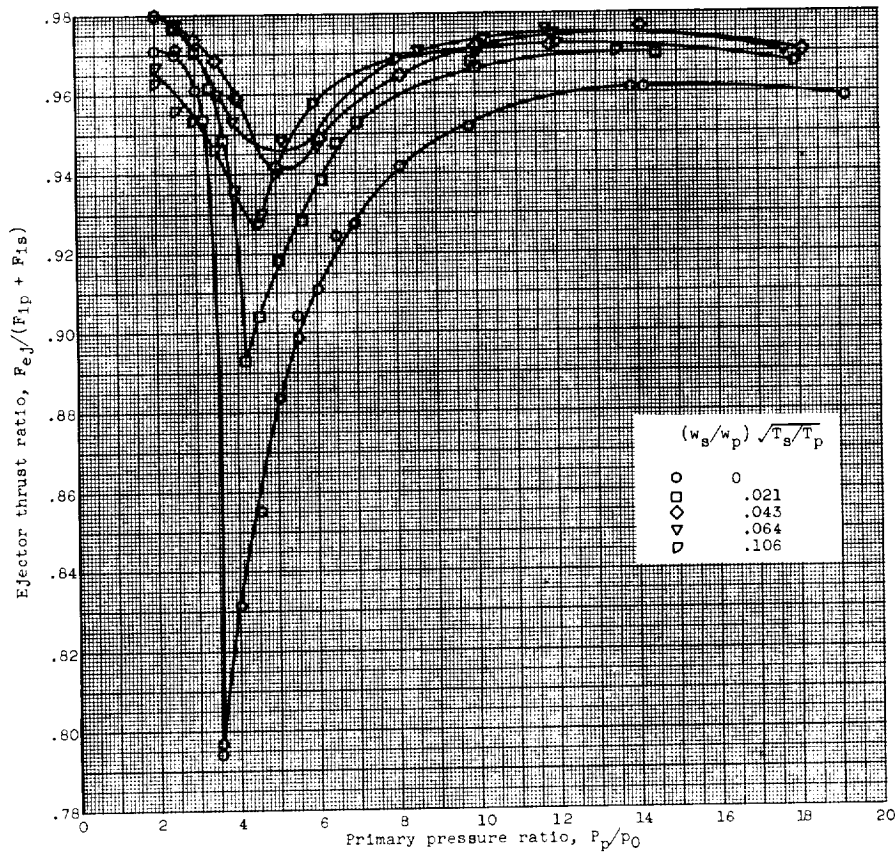




(a) Pumping performance.

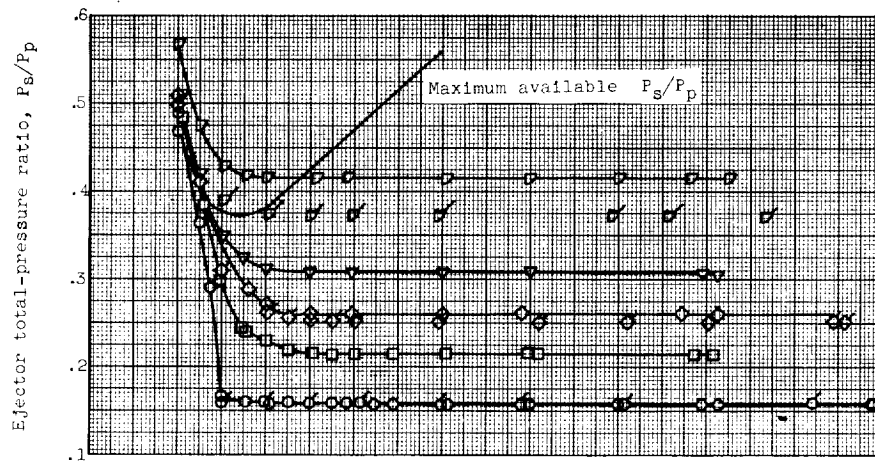


(b) Flow coefficient.

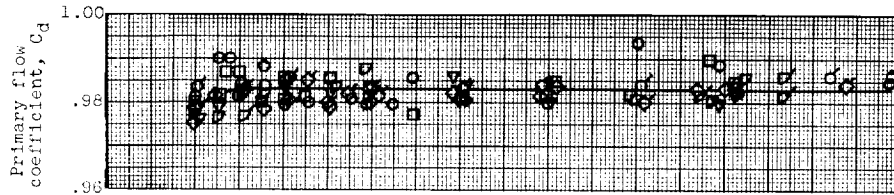


(c) Thrust performance.

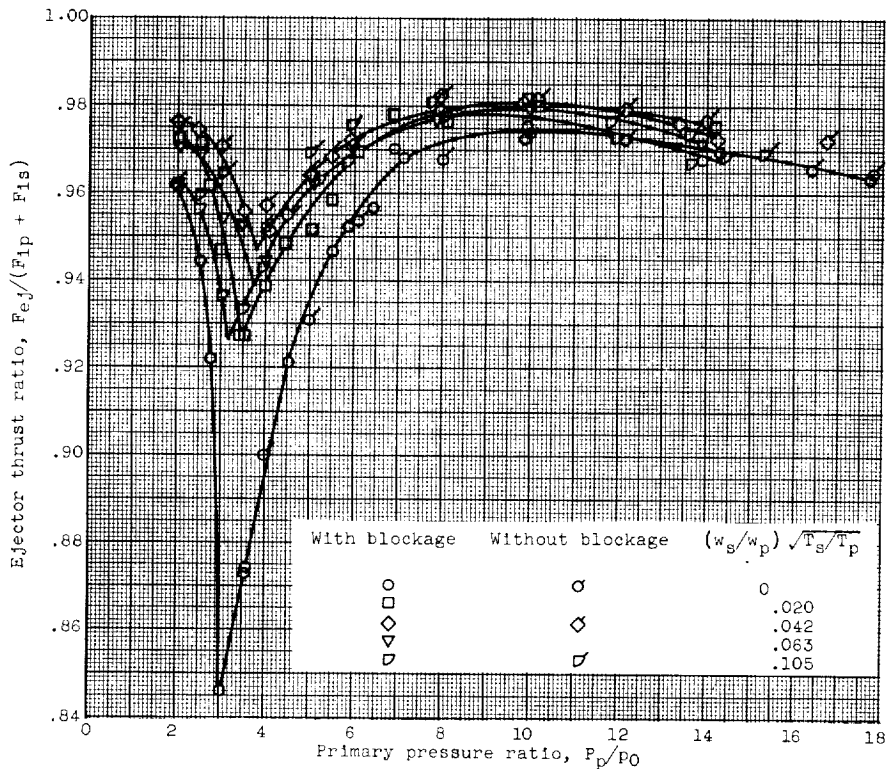
Figure 7. - Performance of configuration 1, maximum afterburning takeoff with secondary blockage. D_p , 8.25 inches; D_e/D_p , 1.50; D_s/D_p , 1.20; L/D_p , 0.93.



(a) Pumping performance.

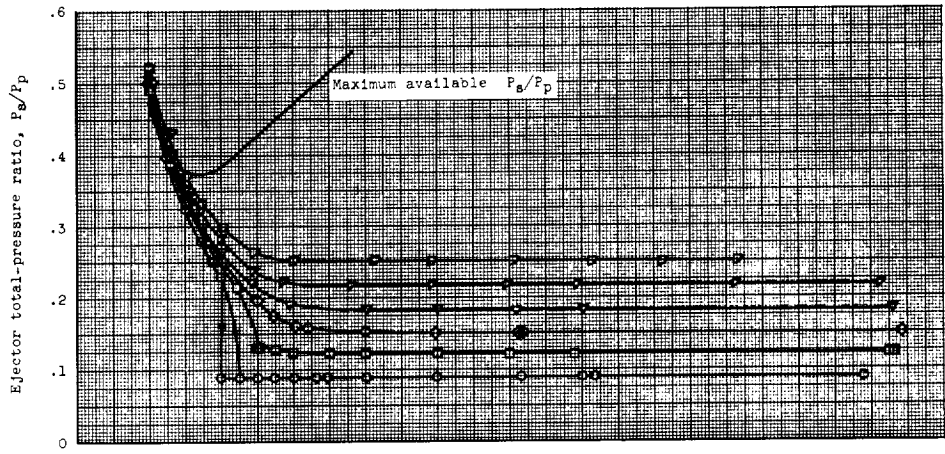


(b) Flow coefficient.

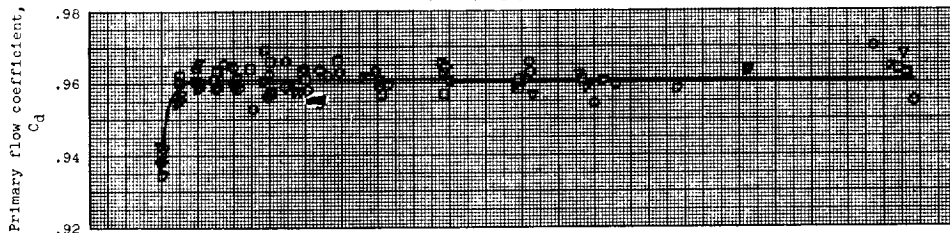


(c) Thrust performance.

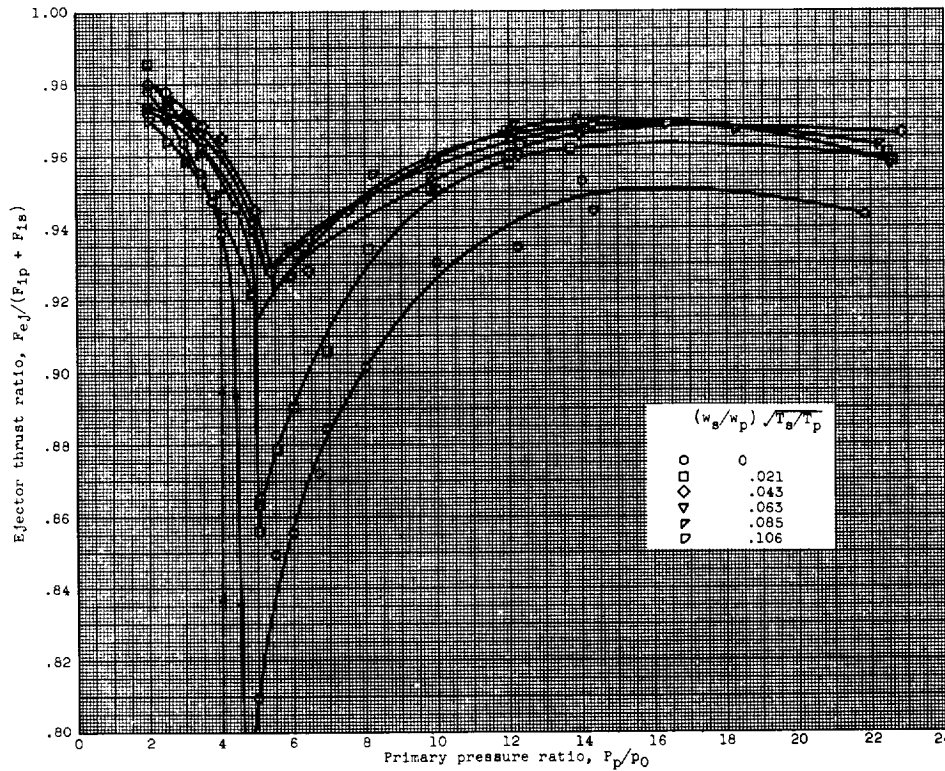
Figure 8. - Performance of configuration 2, maximum afterburning acceleration with and without secondary blockage. D_p , 8.88 inches; D_e/D_p , 1.40; D_s/D_p , 1.11; L/D_p , 0.86.



(a) Pumping performance.

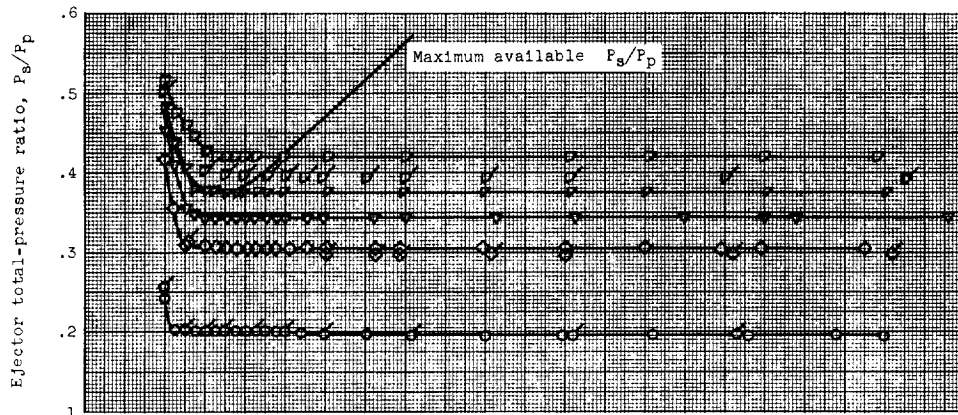


(b) Flow coefficient.

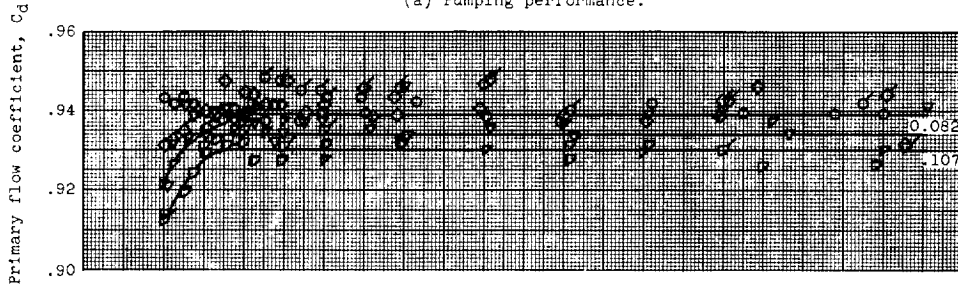


(c) Thrust performance.

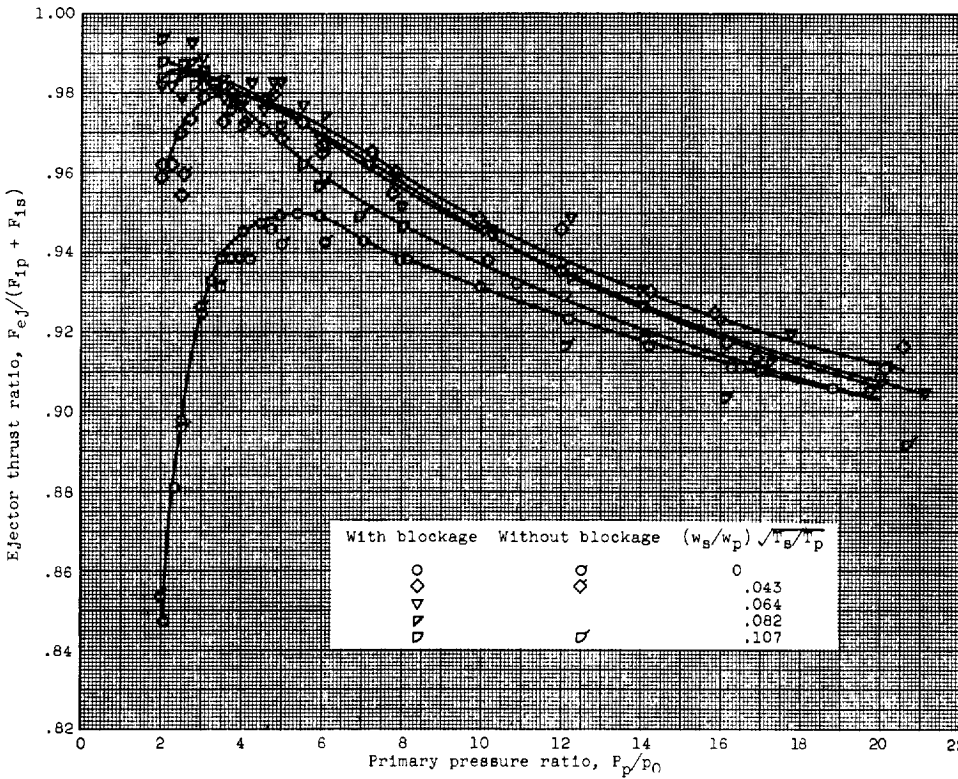
Figure 9. - Performance of configuration 3, partial afterburning cruise with secondary blockage. D_p , 7.58 inches; D_e/D_p , 1.64; D_s/D_p , 1.31; L/D_p , 1.03.



(a) Pumping performance.



(b) Flow coefficient.



(c) Thrust performance.

Figure 10. - Performance of configuration 4, nonafterburning cruise with and without secondary blockage. D_p , 6.47 inches; D_e/D_p , 1.11; D_s/D_p , 1.25; L/D_p , 1.19.

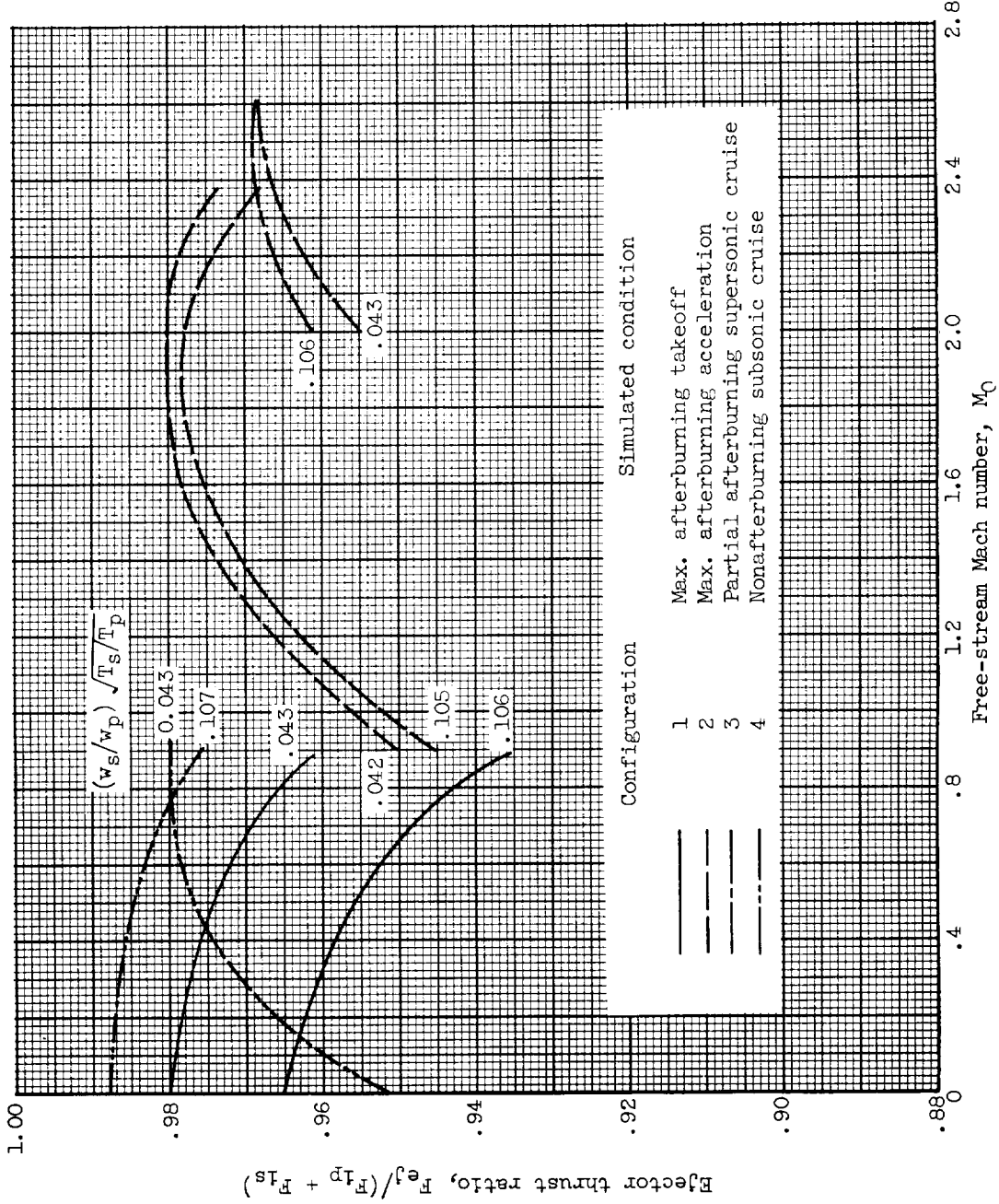


Figure 11. - Composite ejector thrust performance.

